Inorganica Chimica Acta 403 (2013) 78–84

Contents lists available at SciVerse ScienceDirect

Inorganica Chimica Acta

journal homepage: www.elsevier.com/locate/ica

Divalent metal homophthalate coordination polymers with long-spanning dipyridyl ligands containing piperazine moieties

Ciana M. Rogers [b], Curtis Y. Wang [a], Gregory A. Farnum [b], Robert L. LaDuca [b,*]

[a] Diamond Bar High School, Diamond Bar, CA 91765, USA
[b] Lyman Briggs College and Department of Chemistry, Michigan State University, East Lansing, MI 48825, USA

ARTICLE INFO

Article history:
Available online 20 January 2013

Coordination Polymers Special Issue

Keywords:
Zinc
Cobalt
Nickel
Coordination polymer
Luminescence
Magnetism

ABSTRACT

Hydrothermal reaction of a metal nitrate salt, homophthalic acid (H_2hmph), and a long-spanning dipyridyl ligand bearing a central piperazine moiety afforded three new divalent metal homophthalate coordination polymers, which were structurally characterized by single-crystal X-ray diffraction. $[Zn_2(hmph)_2(3\text{-bpmp})]_n$ (**1**, 3-bpmp = bis(3-pyridylmethyl)piperazine) exhibits a 2D (4,4) grid topology formed from the 3-bpmp linkage of $[Zn_2(hmph)_2]_n$ 1D chains featuring$\{Zn_2(OCO)_4\}$ paddlewheel clusters. $\{[Co(H_2O)_4(4\text{-bpfp})][Co(hmph)_2(4\text{-bpfp})]\cdot 6H_2O\}_n$ (**2**, 4-bpfp = bis(4-pyridylformyl)piperazine) possesses alternating anionic $[Co(hmph)_2(4\text{-bpfp})]_n^{2n-}$ and cationic $[Co(H_2O)_4(4\text{-bpfp})]_n^{2n+}$ chains. $[Ni(hmph)(4\text{-bpfp})(H_2O)]_n$ (**3**) manifests $[Ni(H_2O)(hmph)]_n$ chains formed through *anti–syn* carboxylate bridging. In turn these are connected into a (4,4) grid via tethering 4-bpfp ligands. Variable temperature magnetic susceptibility data indicates weak ferromagnetic superexchange along the embedded $[Ni(OCO)]_n$ chain subunits ($g = 2.272(4)$, $J = 0.25(1)$ cm^{-1}). The d^{10} derivative **1** undergoes ligand-centered blue-violet luminescence upon exposure to ultraviolet light ($\lambda_{max} = 417$ nm). Thermal decomposition behavior is also explored.

1. Introduction

The synthesis and characterization of divalent metal benzenedicarboxylate coordination polymers remains an extremely active research focus, as this class of materials has significant potential as gas storage systems [1], selective molecular absorbents [2], ion-exchange substrates [3], heterogeneous catalysts [4], and in non-linear optical applications [5]. The aesthetic appeal of many coordination polymer structures is undeniable, adding to the impetus for further investigations [6].

Aromatic dicarboxylate ligands such as phthalate [7], isophthalate [8], and terephthalate [9], have proven very efficacious in the construction of crystalline coordination polymer solids with functional properties or with unprecedented topologies. By way of example, the 3D interpenetrated phase $[Zn(terephthalate)(4,4'\text{-bpy})_{0.5}]$ (4,4′-bpy = 4,4′-bipyridine) can absorb significant amounts of carbon dioxide [9a]. $[Co(Hphthalate)_2(4,4'\text{-bpy})]_n$ possesses a unique 6-connected self-penetrated 3D network with $5^{10}6^47$ topology built from a diamondoid $[Co(Hphthalate)_2]_n$ subnet with crossing bpy tethers [7a]. Furthermore, the topological scope of these phases can be enhanced by the inclusion of different dipyridyl-type tethering ligands besides the rigid-rod tether 4,4′-bpy. $\{[Cd(phthalate)(dpa)(H_2O)]\cdot 4H_2O\}_n$ (dpa = 4,4′-dipyridylamine) has a simple 4-connected self-penetrated **yyz** net with 7^48^2 topology [7b], while $\{[Cu_2(pht)_2(dpa)]\cdot H_2O\}_n$ has a hexagonal 1D nanotubular structure with open pores [7c]. Thus, metal coordination preference can play a very significant role in instilling the final coordination polymer topology and dimensionality in these dual-ligand systems.

In comparison to the numerous coordination polymers containing short-arm benzenedicarboxylate ligands, related phases containing the potentially more flexible homophthalate ligand (hmph, Scheme 1) are much rarer [10–13]. The extra degrees of conformational freedom can instill diverse coordination polymer topologies in response to the presence of a dipyridyl co-ligand with a particular donor disposition. $\{[Cd(hmph)(4\text{-bpmp})_{1.5}]\cdot 4H_2O\}_n$ (4-bpmp = bis(4-pyridylmethyl)piperazine)) manifests a new 3-fold interpenetrated 5-connected 3D net with a simple 4^46^6 topology, significantly different from the usual, common **sqp** topology. The different steric and supramolecular environment provided by bis(4-pyridylformyl)piperazine (4-bpfp) afforded $[Cd_2(hmph)_2(4\text{-bpfp})]_n$, which displays a rarely encountered 4,5-connected binodal **tcs** net with $(4^46^2)(4^46^6)$ topology [10]. $[Zn_2(hmph)_2(4\text{-bpfp})]_n$ has a decorated (4,4) grid topology with embedded $[Zn_2(OCO)_4]$ paddlewheel clusters [10]. [Cd(hmph)(4,4′-bpy)] shows a simple (4,4) grid topology, and is reported to emit red visible light upon ultraviolet excitation [11], while $\{[Ni(hmph)(dpa)]\cdot 1.33H_2O\}_n$ possesses a (6,3) herringbone grid topology [12].

---

* Corresponding author. Address: Lyman Briggs College, E-30 Holmes Hall, Michigan State University, East Lansing, MI 48825, USA. Tel.: +1 0016168369968.

E-mail address: laduca@msu.edu (R.L. LaDuca).

0020-1693/$ - see front matter © 2013 Elsevier B.V. All rights reserved.
http://dx.doi.org/10.1016/j.ica.2013.01.005

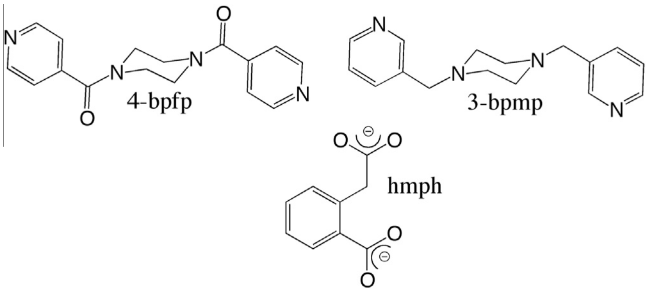

Scheme 1. Ligands used in this study.

In this study we have aimed to extend the presently limited scope of known divalent metal homophthalate long-spanning dipyridyl coordination polymers with the synthesis, structural characterization, and physical property determinations of $[Zn_2(hmph)_2(3\text{-bpmp})]_n$ (**1**), $\{[Co(H_2O)_4(4\text{-bpfp})][Co(hmph)_2(4\text{-bpfp})]\cdot 6H_2O\}_n$ (**2**), and $[Ni(hmph)(4\text{-bpfp})(H_2O)]_n$ (**3**). Luminescent properties are recorded for the d^{10} derivative **1**, while variable temperature magnetic susceptibility experiments were carried out to investigate spin communication between juxtaposted paramagnetic centers in **3**. Thermal decomposition behavior has been probed for all three new materials.

2. Experimental

2.1. General considerations

Metal salts, homophthalic acid, and ligand precursors were obtained from Aldrich. Bis(3-pyridylmethyl)piperazine [14] and bis(4-pyridylformyl)piperazine [15] were prepared using literature procedures. Water was deionized above 3 MΩ-cm in-house. IR spectra were recorded on a Perkin Elmer Spectrum One DRIFT instrument on powdered samples. Elemental Analysis was carried out using a Perkin Elmer 2400 Series II CHNS/O Analyzer. The luminescence spectrum of **1** was obtained with a Hitachi F-4500 Fluorescence Spectrometer on a solid crystalline sample anchored to quartz microscope slides with Rexon Corporation RX-22P ultraviolet-transparent epoxy adhesive. Variable temperature magnetic susceptibility data (2 K to 300 K) for **3** were collected on a Quantum Design MPMS SQUID magnetometer at an applied field of 0.1 T. After each temperature change the sample was kept at the new temperature for 5 min before magnetization measurement to ensure thermal equilibrium. The susceptibility data was corrected for diamagnetism using Pascal's constants [16].

2.2. Preparation of $[Zn_2(hmph)_2(3\text{-bpmp})]_n$ (1)

$Zn(NO_3)_2\cdot 6H_2O$ (42 mg, 0.14 mmol), 3-bpmp (38 mg, 0.14 mmol) and homophthalic acid (25 mg, 0.14 mmol) were placed into 5 mL distilled H_2O in a 15 mL screw-cap vial. The vial was sealed as tightly as possible by hand and heated at 80 °C in an oil bath for 48 h. It was then withdrawn from the oil bath and allowed to air cool to 25 °C. Colorless blocks of **1** (50 mg, 95% yield based on Zn) were isolated after washing with distilled water and acetone, and drying in air. *Anal.* Calc. for $C_{34}H_{32}N_4O_8Zn_2$ **1**: C, 54.06; H, 4.12; N, 5.73. Found: C, 53.52; H, 3.79; N, 5.31%. IR (cm^{-1}): 2921 (m), 2852 (m), 1629 (s), 1598 (m), 1460 (m), 1404 (s), 1300 (w), 1187 (w), 1148 (w), 1064 (w), 1004 (w), 936 (w), 801 (m), 741 (s), 704 (s), 674 (s), 658 (m).

2.3. Preparation of $\{[Co(H_2O)_4(4\text{-bpfp})][Co(hmph)_2(4\text{-bpfp})]\cdot 6H_2O\}_n$ (2)

$Co(NO_3)_2\cdot 6H_2O$ (41 mg, 0.14 mmol), 4-bpfp (41 mg, 0.14 mmol), homophthalic acid (25 mg, 0.14 mmol), and 0.5 mL 1.0 M NaOH were placed into 5 mL distilled H_2O in a 15 mL screw-cap glass vial. The vial was sealed as tightly as possible by hand and heated at 80 °C in an oil bath for 48 h. It was then withdrawn from the oven and allowed to air cool to 25 °C. Orange blocks of **2** (42 mg, 48% yield based on Co) were isolated after washing with distilled water and acetone, and drying in air. *Anal.* Calc. for $C_{25}H_{32}CoN_4O_{11}$ **2**: C, 48.16; H, 5.17; N, 8.99. Found: C, 48.12; H, 5.17; N, 8.86%. IR (cm^{-1}): 3300 (w, br), 2923 (w), 1650 (m), 1603 (m), 1530 (s), 1465 (w), 1433 (m), 1397 (s), 1290 (m), 1260 (m), 1210 (w), 1156 (m), 1053 (w), 1007 (s), 869 (w), 842 (m), 797 (w), 741 (m), 700 (s), 673 (s).

2.4. Preparation of $[Ni(hmph)(4\text{-bpfp})(H_2O)]_n$ (3)

$Ni(NO_3)_2\cdot 6H_2O$ (41 mg, 0.14 mmol), 4-bpfp (41 mg, 0.14 mmol), homophthalic acid (25 mg, 0.14 mmol), and 0.5 mL 1.0 M NaOH were placed into 5 mL distilled H_2O in a 15 mL screw-cap glass vial. The vial was sealed as tightly as possible by hand and heated at 80 °C in an oil bath for 48 h. Blue needles of **3** (67 mg, 87% yield based on Ni) were isolated after washing with distilled water and acetone, and drying in air. *Anal.* Calc. for $C_{25}H_{24}N_4NiO_7$ **3**: C, 54.48; H, 4.39; N, 10.16. Found: C, 53.74; H, 4.38; N, 9.80%. IR (cm^{-1}): 3500 (w, br), 2961 (w), 1660 (m), 1614 (m), 1582 (m), 1561 (s), 1547 (s), 1412 (s), 1385 (s), 1289 (m), 1260 (s), 1221 (w), 1151 (w), 1086 (w), 1050 (w), 1003 (s), 842 (m), 790 (m), 777 (w), 767 (w), 735 (s), 709 (s), 663 (s).

3. X-ray crystallography

Single crystal reflection data for **1**–**3** were collected at 173 K using a Bruker-AXS Apex II CCD instrument. Reflection data was acquired using graphite-monochromated Mo Kα radiation ($\lambda = 0.71073$ Å). The data was integrated via SAINT [17]. Lorentz and polarization effect and absorption corrections were applied with SADABS [18]. The structures were solved using direct methods and refined on F^2 using SHELXTL [19]. All non-hydrogen atoms were refined anisotropically. Hydrogen atoms bound to carbon atoms were placed in calculated positions and refined isotropically with a riding model. Where possible, hydrogen atoms belonging to water molecules were found by Fourier difference map and refined with isotropic thermal displacement parameters. Relevant crystallographic data for **1**–**3** are listed in Table 1.

4. Results and discussion

4.1. Synthesis and spectral characterization

Compounds **1**–**3** were prepared by the hydrothermal reaction of the appropriate metal salt, homophthalic acid, and the requisite dipyridyl ligand, with the addition of aqueous base for **2**–**3**. The infrared spectra of all of the compounds were consistent with their crystal structures.

Weak, highly broadened features above ~3200 cm^{-1} in the spectrum of **2** and **3** indicate the presence of the bound and/or unligated water molecules. Bands between 2800 and 3100 cm^{-1} in all spectra represent C–H stretching modes. Asymmetric and symmetric C–O stretching modes of the hmph ligands are present as broadened, stronger bands at 1629 and 1404 cm^{-1} (**1**), and 1530 and 1397 cm^{-1} (**2**), 1561 and 1385 cm^{-1} for the monodentate carboxylate group in **3**, and 1547 and 1412 cm^{-1} for the bridging carboxylate group in **3**. A narrower $\Delta\nu$ gap between the C–O stretching bands has been ascribed to a bridging or chelating carboxylate binding mode [20]. Medium intensity bands in the range of ~1600 to ~1200 cm^{-1} are caused by stretching modes of the pyridyl rings of the 3-bpmp or 4-bpfp ligands and the aromatic

Table 1
Crystal and structure refinement data for **1**–**3**.

Data	1	2	3
Empirical Formula	$C_{34}H_{32}N_4O_8Zn_2$	$C_{25}H_{32}CoN_4O_{11}$	$C_{25}H_{24}N_4NiO_7$
Formula weight	755.38	623.48	551.19
Crystal system	triclinic	triclinic	monoclinic
Space group	$P\bar{1}$	$P\bar{1}$	$P2_1/c$
a (Å)	7.775(2)	7.4031(9)	16.411(3)
b (Å)	10.371(3)	11.9709(14)	16.687(3)
c (Å)	10.484(3)	16.4265(19)	8.7009(16)
α (°)	92.643(3)	97.706(1)	90
β (°)	107.411(3)	96.661(1)	91.587(2)
γ (°)	106.529(4)	100.489(1)	90
V (Å^3)	765.3(4)	1365.0(3)	2381.9(8)
Z	1	2	4
D_{calc} (g cm^{-3})	1.639	1.517	1.537
μ (mm^{-1})	1.629	0.696	0.870
Min./max. transmission	0.6997/0.8807	0.7557/0.8744	0.7488/0.9777
hkl ranges	$-10 \leqslant h \leqslant 10$, $-13 \leqslant k \leqslant 13$, $-13 \leqslant l \leqslant 13$	$8 \leqslant h \leqslant 8$, $-14 \leqslant k \leqslant 14$, $-19 \leqslant l \leqslant 19$	$19 \leqslant h \leqslant 19$, $0 \leqslant k \leqslant 20$, $0 \leqslant l \leqslant 10$
Total reflections	13340	22162	50075
Unique reflections	3615	4958	4365
R_{int}	0.0474	0.0261	0.1171
Parameters/restraints	217/0	403/15	340/3
R_1[a] (all data)	0.0452	0.0271	0.0930
R_1[a] ($I > 2\sigma(I)$)	0.0335	0.0243	0.0643
wR_2[b] (all data)	0.0784	0.0620	0.1647
wR_2[b] ($I > 2\sigma(I)$)	0.0731	0.0601	0.1507
Max/min residual (e$^-$/Å^3)	0.393/−0.342	0.270/−0.303	0.584/−1.074
Goodness-of-fit (GOF) on F^2	1.043	1.045	1.117

[a] $R_1 = \Sigma||F_o| - |F_c||/\Sigma|F_o|$.
[b] $wR_2 = \{\Sigma [w(F_o^2 - F_c^2)^2]/\Sigma [wF_o^2]^2\}^{1/2}$.

rings of the hmph ligands [21]. The C–O carbonyl stretching bands of the 4-bpfp ligands appeared at 1650 cm^{-1} (**2**) or 1660 cm^{-1} (**3**).

4.2. Structural description of $[Zn_2(hmph)_2(3\text{-bpmp})]_n$ (*1*)

The asymmetric unit of compound **1** contains a divalent zinc atom, a fully deprotonated hmph dianion, and half of a 3-bpmp ligand whose piperazinyl ring centroid is situated at a crystallographic inversion center. A slightly distorted $\{ZnO_4N\}$ square pyramidal coordination environment is present in **1** (Fig. 1a); the zinc atom rests 0.35 Å above the plane defined by the four hmph oxygen donor atoms in the equatorial positions. Two of these, in *trans* positions, are provided by short hmph carboxylate arms. The other two *trans* oxygen donors belong to long hmph carboxylate pendant arms. The axial position is taken up by a pyridyl nitrogen donor atom from a 3-bpmp ligand. Bond lengths and angles within the coordination environment are listed in Table 2.

Exotetradentate hmph ligands with a μ_4-κ^4O:O′:O″:O‴ binding mode (Scheme 2) produce $[Zn_2(hmph)_2]_n$ 1D coordination polymer chains aligned along the *a* crystallographic axis, with embedded $\{Zn_2(OCO)_4\}$ paddlewheel dimeric units (Fig. 1b). The Zn···Zn through space distance across the dimeric kernel is 2.9258(9) Å; the related distance across the hmph ligand is 7.775 Å, defining the *a* lattice parameter. Parallel $[Zn_2(hmph)_2]_n$ chain motifs are linked into $[Zn_2(hmph)_2(3\text{-bpmp})]_n$ 2D coordination polymer layers (Fig. 1c) by *anti*-conformation 3-bpmp ligands. These layers lie parallel to the $(01\bar{1})$ crystal planes. The Zn···Zn internuclear distance through the 3-bpmp ligands is 14.097 Å. Very similar dimer-bearing $[Zn_2(hmph)_2]_n$ chains were seen in the related phase $[Zn_2(hmph)_2(4\text{-bpfp})]_n$ [10].

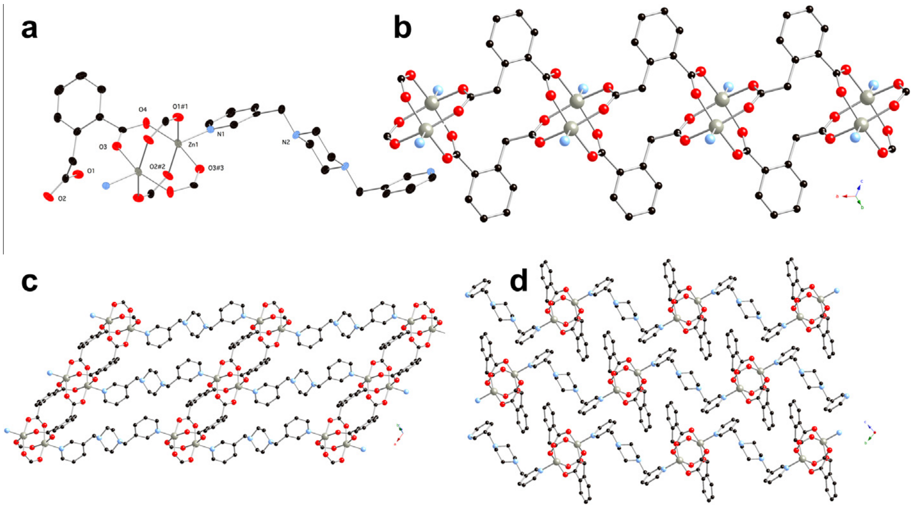

Fig. 1. (a) Coordination environment at Zn in **1**. (b) $[Zn_2(hmph)_2]_n$ 1D chain in 1. (c) $[Zn_2(hmph)_2(3\text{-bpmp})]_n$ layer in **1**. (d) Stacking of $[Zn_2(hmph)_2(3\text{-bpmp})]_n$ layers.

Table 2
Selected bond distance (Å) and angle (°) data for **1**.

Zn1–N1	2.0274(19)
Zn1–O1$^{\#1}$	2.0393(17)
Zn1–O2$^{\#2}$	2.0403(17)
Zn1–O4	2.0443(17)
Zn1–O3$^{\#3}$	2.0704(16)
N1–Zn1–O1$^{\#1}$	100.20(7)
N1–Zn1–O2$^{\#2}$	99.21(7)
O1$^{\#1}$–Zn1–O2$^{\#2}$	160.45(7)
N1–Zn1–O4	103.18(7)
O1$^{\#1}$–Zn1–O4	90.51(8)
O2$^{\#2}$–Zn1–O4	87.29(8)
N1–Zn1–O3$^{\#3}$	96.40(7)
O1$^{\#1}$–Zn1–O3$^{\#3}$	85.48(7)
O2$^{\#2}$–Zn1–O3$^{\#3}$	90.11(7)
O4–Zn1–O3$^{\#3}$	160.41(7)

Symmetry equivalent positions: #1 $x-1, y, z$; #2 $-x+1, -y-2, -z-1$; #3 $-x, -y-2, -z-1$.

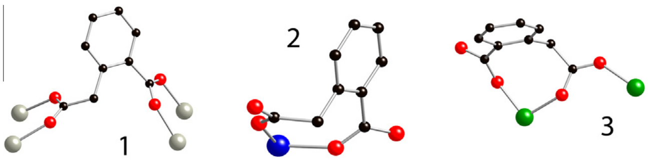

Scheme 2. Binding modes of the homophthalate ligands in **1**–**3**.

If each $\{Zn_2(OCO)_4\}$ paddlewheel dimer in **1** is treated as a 4-connected node, the layer structure can be considered a simple (4,4) grid. Adjacent $[Zn_2(hmph)_2(3\text{-bpmp})]_n$ layers stack in an *AAA* pattern along both the *b* and *c* directions via three different interlayer interactions: non-classical C–H···O interactions, π–π stacking between hmph aromatic rings, and π–π stacking between 3-bpmp pyridyl rings (Fig. 1d).

4.3. Structural description of $\{[Co(H_2O)_4(4\text{-bpfp})][Co(hmph)_2(4\text{-bpfp})]\cdot 6H_2O\}_n$ (**2**)

The asymmetric unit of compound **2** contains two divalent cobalt atoms (Co1, Co2) on crystallographic inversion centers, two aqua ligands, a hmph ligand, halves of two crystallographically distinct 4-bpfp ligands whose piperazinyl ring centroids are situated on inversion centers, and three water molecules of crystallization. Both Co1 and Co2 exhibit a $\{CoO_4N_2\}$ octahedral coordination sphere with *trans* pyridyl nitrogen donor atoms from 4-bpfp ligands. Co1 possesses two sets of *cis* hmph carboxylate oxygen atom donors, in which both *cis* oxygen donors arise from the same hmph ligand. Therefore the hmph ligands in **2** do not bridge metal centers, but instead bind to a single cobalt atom with a chelating $\kappa^2O:O''$ binding mode (Scheme 2). Donors from the long carboxylate pendant arms of two hmph ligands are disposed in a *trans* manner, as are donors from the short carboxylate arms (Fig. 2a). On the other hand, the coordination environment of Co2 shows four aqua ligands in its equatorial plane (Fig. 2b). Metrical parameters within the coordination spheres are given in Table 3.

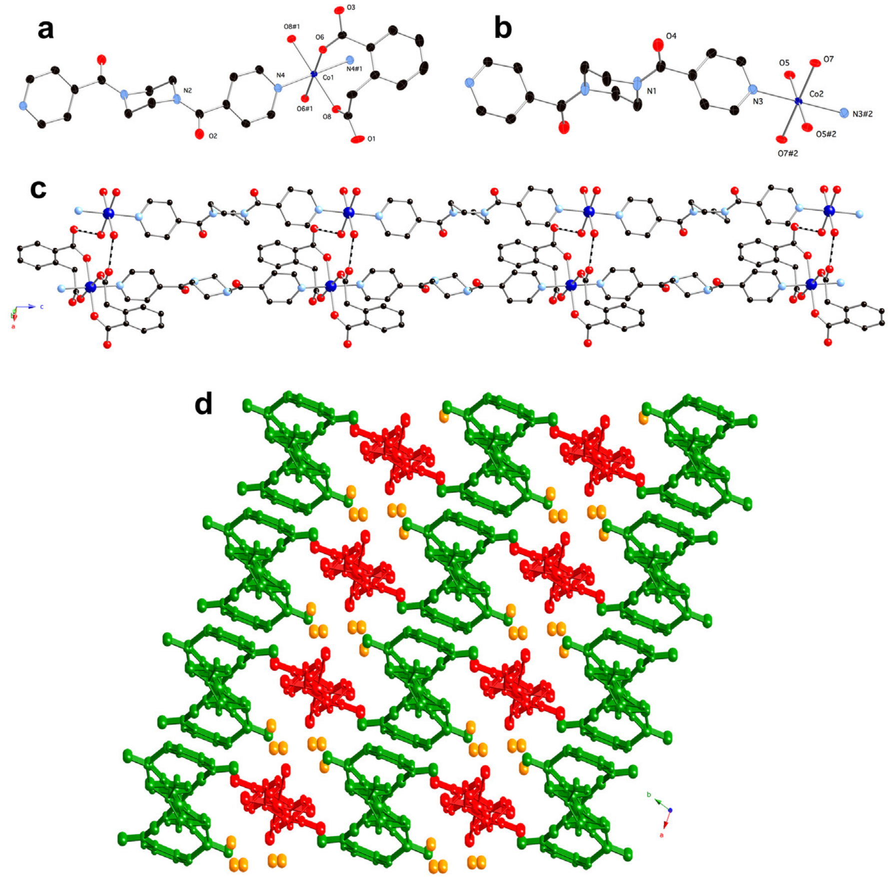

Fig. 2. (a) Coordination environment at Co1 in **2**. (b) Coordination environment at Co2 in **2**. (c) Hydrogen-bonded pair of $[Co(hmph)_2(4\text{-bpfp})]_n^{2n-}$ anionic chain and $[Co(H_2O)_4(4\text{-bpfp})]_n^{2n+}$ cationic chain in **2**. Hydrogen bonding is shown as dashed lines. (d) Stacking diagram for **2**, with anionic chain motifs in green and cationic chain motifs in red. The colors refer to the graphic in the online version of this article.

Table 3
Selected bond distance (Å) and angle (°) data for **2**.

Co1–O6	2.0430(10)	O8–Co1–N4	89.62(4)
Co1–O8	2.1441(10)	O6$^{\#1}$–Co1–N4	90.39(4)
Co1–N4	2.1471(12)	N4–Co1–N4$^{\#1}$	180.0
Co2–O7	2.0512(11)	O7$^{\#2}$–Co2–O7	180.0
Co2–O5	2.1059(11)	O7$^{\#2}$–Co2–O5	90.12(4)
Co2–N3	2.1622(13)	O7–Co2–O5	89.88(4)
O6–Co1–O6$^{\#1}$	180.0	O5$^{\#2}$–Co2–O5	180.0
O6–Co1–O8	96.01(4)	O7$^{\#2}$–Co2–N3	89.68(5)
O6$^{\#1}$–Co1–O8	83.99(4)	O7–Co2–N3	90.32(5)
O8–Co1–O8$^{\#1}$	180.0	O5$^{\#2}$–Co2–N3	92.34(5)
O6–Co1–N4	90.98(4)	O5–Co2–N3	87.66(5)
O6$^{\#1}$–Co1–N4	89.02(4)	N3$^{\#2}$–Co2–N3	180.0

Symmetry equivalent positions: #1 $-x+1, -y+1, -z$; #2 $-x+2, -y, -z$.

The anionic $[Co(hmph)_2]^{2-}$ fragments based on Co1 are linked into anionic $[Co(hmph)_2(4\text{-bpfp})]_n^{2n-}$ chains by *anti*-conformation 4-bpfp ligands. Similarly, cationic $[Co(H_2O)_4]^{2+}$ fragments are connected into $[Co(H_2O)_4(4\text{-bpfp})]_n^{2n+}$ chains by other *anti*-conformation 4-bpfp ligands. In both chain motifs, the through-ligand Co···Co distance is 16.427 Å, defining the *c* lattice parameter. Pairs of distinct coordination polymer chains are connected to each other via hydrogen bonding between the aqua ligands in the cationic chains and ligated or unligated hmph carboxylate oxygen atoms in the anionic chains (Fig. 2c). Trapped between pairs of chains of each type, in 1D incipient channels, lie co-crystallized water molecule trimers (Fig. 2d). These are held to the coordination polymer chains by hydrogen bonding patterns involving hmph carboxylate oxygen atoms and aqua ligands (Table 4).

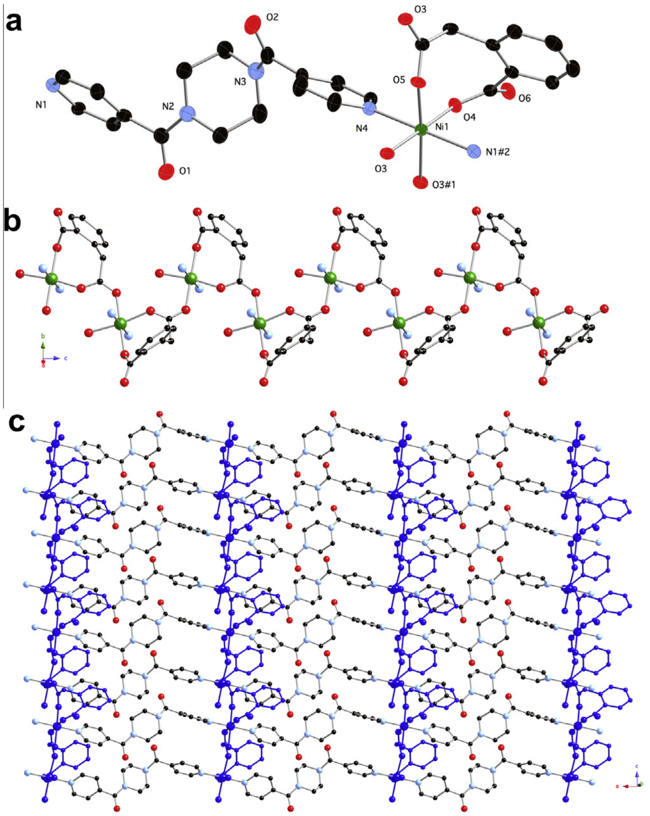

Fig. 3. (a) Coordination environment at Ni in **3**. (b) $[Ni(H_2O)(hmph)]_n$ chain in **3**, featuring *anti–syn* bridged $[Ni(OCO)]_n$ chain subunit. (c) $[Ni(H_2O)(hmph)(4\text{-bpfp})]_n$ layers with $[Ni(H_2O)(hmph)]_n$ chains drawn in blue (online version of the article).

4.4. Structural description of $[Ni(hmph)(4\text{-bpfp})(H_2O)]_n$ (**3**)

The asymmetric unit of compound **3** contains a divalent nickel atom, a hmph ligand, a 4-bpfp ligand, and an aqua ligand. Nickel atoms in **3** display a $\{NiO_4N_2\}$ octahedral coordination environment, with *trans* pyridyl nitrogen donors from two 4-bpfp ligands (Fig. 3a). Two carboxylate oxygen atoms from a single hmph ligand occupy cis coordination sites in the equatorial plane. The other two equatorial sites are filled by an aqua ligand and a carboxylate oxygen atom from a second hmph ligand. Bond lengths and angles within the coordination environment in **3** are given in Table 5.

Dissimilar to the exotetradentate binding mode in **1** and the chelating binding mode in **2**, the hmph ligands in **3** adopt an exobidentate μ^2-$\kappa^3O,O'':O'''$ binding mode (Scheme 2). Both the short and long carboxylate arms of the hmph ligand chelate to a single nickel atom, while the long carboxylate arm also binds to another nickel atom. Via this binding mode, $[Ni(H_2O)(hmph)]_n$ 1D coordination polymer chains are formed in which neighboring nickel atoms are linked by carboxylate groups in an *anti–syn* fashion (Fig. 3b). The Ni···Ni distance along the embedded $[Ni(OCO)]_n$ chain subunits is 5.265 Å. Parallel $[Ni(H_2O)(hmph)]_n$ chains are aligned along the *c* crystallographic direction.

Neighboring $[Ni(H_2O)(hmph)]_n$ chains are connected into $[Ni(H_2O)(hmph)(4\text{-bpfp})]_n$ (4,4) coordination polymer grids (Fig. 3c) by tethering 4-bpfp ligands with a slightly twisted *anti* conformation (O···N···N···O torsion angle = 152.2°). The Ni···Ni distance across the 4-bpfp within the coordination polymer grid is 16.411 Å, marking the *a* lattice parameter. Supramolecular π–π stacking between hmph aromatic rings and 3-bpmp pyridyl rings serves an ancillary structure stabilization role within the layers. Adjacent $[Ni(H_2O)(hmph)(4\text{-bpfp})]_n$ layers stack in an *ABAB* pattern along the c crystal axis, anchored to each other through hydrogen

Table 4
Hydrogen bonding distance (Å) and angle (°) data for **2**–**3**.

D–H···*A*	*d*(H···*A*)	∠*DHA*	*d*(*D*···*A*)	Symmetry transformation for *A*
2				
O1W–H1WA···O5	2.106(17)	159(2)	2.9160(17)	$x-1, y, z$
O1W–H1WB···O3	1.900(17)	161(2)	2.7225(17)	$x-1, y-1, z$
O2W–H2WA···O1W	1.890(17)	170(3)	2.746(2)	
O2W–H2WB···O2	1.995(17)	174(3)	2.8370(19)	$x, y-1, z$
O3W–H3WA···O2W	1.94(2)	161(3)	2.759(2)	$-x+1, -y+1, -z+1$
O3W–H3WB···O2	2.13(2)	159(3)	2.926(2)	
O5–H5A···O1	1.780(14)	169.8(18)	2.6168(15)	$x+1, y, z$
O5–H5B···O1	1.860(15)	165.4(18)	2.6780(16)	$-x+2, -y, -z$
O7–H7C···O3	1.826(15)	171.2(18)	2.6627(16)	$x, y-1, z$
O7–H7D···O8	1.914(14)	174.3(18)	2.7635(15)	$-x+1, -y, -z$
3				
O7–H7C···O3	2.73(5)	103(3)	3.041(4)	$x, -y+1/2, z-1/2$
O7–H7D···O5	2.00(2)	155(4)	2.814(4)	$x, -y+1/2, z-1/2$

Table 5
Selected bond distance (Å) and angle (°) data for **3**.

Ni1–O5	2.053(3)	$O3^{\#1}$–Ni1–O7	94.76(12)
Ni1–O4	2.064(3)	O5–Ni1–$N1^{\#2}$	91.05(13)
Ni1–$O3^{\#1}$	2.065(3)	O4–Ni1–$N1^{\#2}$	90.60(13)
Ni1–O7	2.068(3)	$O3^{\#1}$–Ni1–$N1^{\#2}$	89.71(13)
Ni1–$N1^{\#2}$	2.091(4)	O7–Ni1–$N1^{\#2}$	87.94(13)
Ni1–N4	2.092(4)	O5–Ni1–N4	89.98(13)
O5–Ni1–O4	101.97(12)	O4–Ni1–N4	88.09(13)
O5–Ni1–$O3^{\#1}$	77.30(11)	$O3^{\#1}$–Ni1–N4	91.61(13)
O4–Ni1–$O3^{\#1}$	179.21(12)	O7–Ni1–N4	91.19(13)
O5–Ni1–O7	172.00(12)	$N1^{\#2}$–Ni1–N4	178.48(14)
O4–Ni1–O7	85.98(12)		

Symmetry equivalent positions: #1 *x*, $-y + 1/2$, $z - 1/2$; #2 $x - 1$, *y*, *z*.

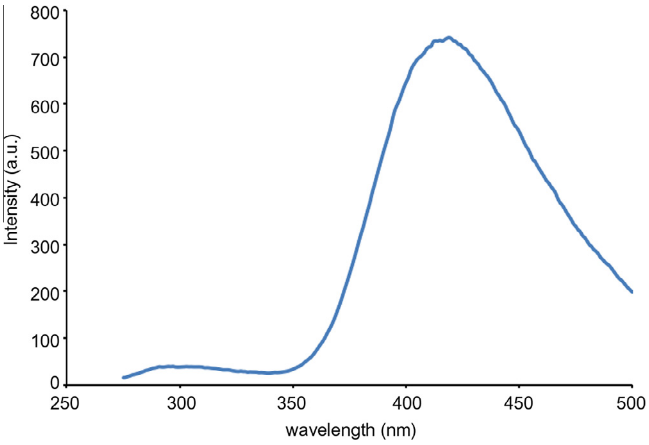

Fig. 4. Emission spectrum of **1**.

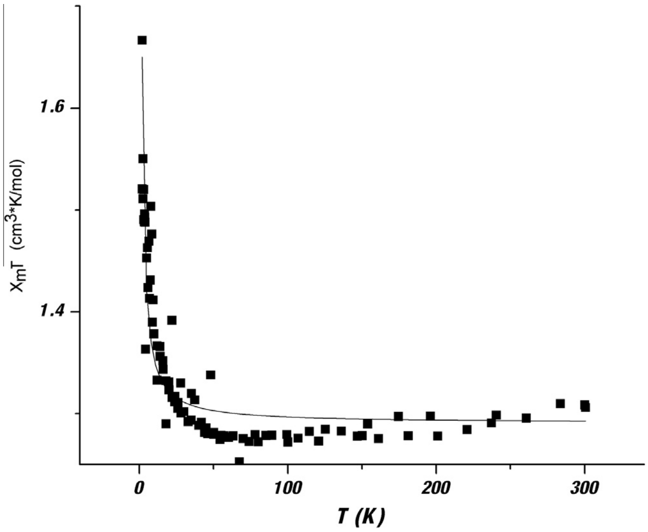

Fig. 5. Variable temperature magnetic susceptibility data for **3**. The best fit to Eq. (1) is shown as a thin black line.

bonding donation from aqua ligands to unligated long hmph carboxylate group oxygen atoms (Table 4).

4.5. Luminescent properties of 1

Irradiation of a crystalline sample of complex **1** with ultraviolet light ($\lambda_{ex} = 260$ nm) caused moderately intense blue-violet visible light emission with a maximum at $\lambda = 418$ nm (Fig. 4). This emission profile matches reasonably well with that of free homophthalic acid (445 nm), while 3-bpmp showed very weak luminescence under the same excitation wavelength. Via comparison with other d^{10} metal coordination polymers with aromatic ligands [22], the emissive properties of **1** likely arises from ligand-centered $\pi-\pi$ or $\pi-n$ molecular orbital electronic transitions within the phenyl rings of the hmph ligands. The blueshift of the emission maximum is likely caused by coordination of the hmph ligand to zinc.

4.6. Magnetic properties of 3

A variable temperature magnetic susceptibility experiment was carried out in order to investigate spin communication along the embedded $[Ni(OCO)]_n$ chain subunits in **3**. A Curie–Weiss plot over the entire temperature range (Fig. S1) gives $C = 1.29$ cm^3 K mol^{-1} and $\Theta = 0.06$ K, with the small, positive Θ value portending weak ferromagnetic coupling. At 300 K, the χ_mT product was 1.30 cm^3 K mol^{-1}, somewhat higher than expected for an isolated $S = 1$ Ni^{2+} ion (1.00 cm^3 K mol^{-1}), indicative of possible ferromagnetic coupling. This value remained largely steady upon cooling to 40 K. Below this temperature, χ_mT product increased more rapidly, thus corroborating the presence of ferromagnetic superexchange through the *anti–syn* carboxylate bridges. Fitting of the data (Fig. 5) to Fisher's expression [23] for a 1D chain of $S = 1$ ions Eq. (1) gives $g = 2.272(4)$ and $J = 0.25(1)$ cm^{-1} with $R = \{\Sigma\, [(\chi_mT)_{obs} - (\chi_mT)_{calc}]^2\}^{1/2} = 1.23 \times 10^{-3}$. The small, positive *J* value also indicates weak ferromagnetic coupling of e_g-like orbital unpaired electrons through the carboxylate molecular orbitals.

$$\begin{aligned} \chi_m T &= \left(\frac{Ng^2\beta^2 S(S+1)}{3k}\right)\left(\frac{1+u}{1-u}\right) \\ u &= \coth\left[\frac{JS(S+1)}{kT}\right] - \left[\frac{kT}{JS(S+1)}\right] \end{aligned} \qquad (1)$$

4.7. Thermal properties

Thermogravimetric analysis was undertaken to examine the decomposition behavior of **1**–**3**. Thermograms are shown in Figs. S2–S4. The thermal degradation of compound **1** began at 135 °C via likely decarboxylation of the hmph ligands (11.7% calc'd, 12.8% obs'd), followed by ejection of the 3-bpmp ligands above 290 °C (35.5% calc'd, 39.9% obs'd). The final mass remnant of 26.8% at 475 °C is likely a mixture of ZnO (21.6% calc'd) and some uncombusted organic material. Dehydration of compound **2** occurred between 25 and 85 °C, with a 11.7% mass loss roughly consistent with removal of most of the bound and all of the unbound water molecules (14.4% calc'd). The remainder of the aqua ligands were removed between 85 and 200 °C. Above 250 °C, the organic ligands were ejected from the coordination polymer structure. The final mass remnant of 32.8% at 475 °C is most likely a mixture of $CoCO_3$ (18.9% calc'd) and a fair amount of uncombusted organic material. Compound **3** underwent slow dehydration via ejection of bound water molecules between 25 and 250 °C, with the 3.3% mass loss matching the predicted value for one molar equivalent of water per nickel. Ligand combustion above 250 °C was marked by a precipitous mass loss. The final remnant of 24.6% at 475 °C is likely a combination of $NiCO_3$ (21.4% calc'd) and a small amount of uncombusted carbonaceous material.

5. Conclusions

Related, long-spanning dipyridyl/piperazine ligands have afforded new divalent coordination polymers with the seldom used flexible-arm homophthalate ligand, thereby expanding the scope of its coordination polymer structural chemistry. Using the kinked-disposition 3-bpmp ligand gave a coordination polymer with $[Zn(homophthalate)]_n$ layers featuring $\{Zn_2(OCO)_4\}$ paddlewheel dimers, very similar to the structure of a previously synthesized zinc homophthalate derivative. Differences in homophthalate binding mode and affinity for aqua ligands promoted structural diversity in nickel and cobalt materials containing a related dipyridyl/piperazine ligand bearing formyl groups. A large number of aqua ligands in the cobalt case afforded a 1D coordination polymer system in **2**. Fewer aqua ligands in the nickel derivative **3** allowed a bridging binding mode for homophthalate carboxylate groups, resulting in an increase in dimensionality and spin communication along weakly ferromagnetically coupled embedded $[Ni(OCO)]_n$ chains. Aromatic-ligand centered luminescent properties were observed as expected for the zinc homophthalate coordination polymer.

Acknowledgements

The authors gratefully acknowledge the donors of the American Chemical Society Petroleum Research fund for financial support of this work. We thank Ms Julie Wilson and Mr Jacob Uebler for experimental assistance.

Appendix A. Supplementary material

CCDC 904801, 904799, and 904800 contain the supplementary crystallographic data for **1**–**3**. These data can be obtained free of charge from The Cambridge Crystallographic Data Centre via http://www.ccdc.cam.ac.uk/data_request/cif. Supplementary data associated with this article can be found, in the online version, at http://dx.doi.org/10.1016/j.ica.2013.01.005.

References

[1] L.J. Murray, M. Dinca, J.R. Long, Chem. Soc. Rev. 38 (2009) 1294 (and references therein).
[2] J.R. Li, R.J. Kuppler, H.C. Zhou, Chem. Soc. Rev. 38 (2009) 1477 (and references therein).
[3] (a) M. Plabst, L.B. McCusker, T. Bein, J. Am. Chem. Soc. 131 (2009) 18112;
(b) Y. Liu, V.C. Kravtsov, M. Eddaoudi, Angew. Chem., Int. Ed. 47 (2008) 8446;
(c) F. Nouar, J. Eckert, J.F. Eubank, P. Forster, M. Eddaoudi, J. Am. Chem. Soc. 131 (2009) 2864.
[4] (a) J. Lee, O.K. Farha, J. Roberts, K.A. Scheidt, S.T. Nguyen, J.T. Hupp, Chem. Soc. Rev. 38 (2009) 1450 (and references therein);
(b) L. Ma, C. Abney, W. Lin, Chem. Soc. Rev. 38 (2009) 1248 (and references therein).
[5] (a) S. Zang, Y. Su, Y. Li, Z. Ni, Q. Meng, Inorg. Chem. 45 (2006) 174;
(b) L. Wang, M. Yang, G. Li, Z. Shi, S. Feng, Inorg. Chem. 45 (2006) 2474.
[6] S.R. Batten, R. Robson, Angew. Chem., Int. Ed. 37 (1998) 1460.
[7] (a) P. Lightfoot, A. Snedden, J. Chem. Soc., Dalton Trans. (1999) 3549;
(b) E. Shyu, R.M. Supkowski, R.L. LaDuca, Inorg. Chem. 48 (2009) 2723;
(c) M.A. Braverman, J.H. Nettleman, R.M. Supkowski, R.L. LaDuca, Inorg. Chem. 48 (2009) 4918.
[8] (a) M. Eddaoudi, J. Kim, N. Rosi, D. Vodak, J. Wachter, M. O'Keefee, O.M. Yaghi, Science 295 (2002) 469;
(b) X.-N. Cheng, W.-X. Zhang, Y.-Y. Lin, Y.-Z. Zheng, X.-M. Chen, Adv. Mater. 19 (2007) 1494.
[9] (a) L. Bastin, P.S. Barcia, E.J. Hurtado, J.A.C. Silva, A.E. Rodrigues, B. Chen, J. Phys. Chem. C 112 (2008) 1575;
(b) H. Li, M. Eddaoudi, M. O'Keeffe, O.M. Yaghi, Nature 402 (1999) 276;
(c) Z. Huang, M. Drillon, N. Masciocchi, A. Sironi, J. Zhao, P. Rabu, P. Panissod, Chem. Mater. 12 (2000) 2805;
(d) X. Wang, C. Qin, Y. Lan, K. Shao, Z. Su, E. Wang, Chem. Commun. (2009) 410.
[10] G.A. Farnum, C.Y. Wang, R.L. LaDuca, Inorg. Chim. Acta 375 (2011) 280.
[11] J. He, Y. Wang, W. Bi, Y. Wang, R. Cao, Polyhedron 25 (2006) 1239.
[12] M.A. Braverman, R.J. Staples, R.M. Supkowski, R.L. LaDuca, Polyhedron 27 (2008) 2291.
[13] J. He, Y. Wang, W. Bi, X. Zhu, R. Cao, J. Mol. Struct 787 (2006) 63.
[14] Y. Niu, H. Hou, Y. Wei, Y. Fan, Y. Zhu, C. Du, X. Xin, Inorg. Chem. Commun. 4 (2001) 358.
[15] H. Hou, Y. Song, H. Xu, Y. Wei, Y. Fan, Y. Zhu, L. Li, C. Du, Macromolecules 36 (2003) 999.
[16] O. Kahn, Molecular Magnetism, VCH Publishers, New York, 1993.
[17] SAINT, Software for Data Extraction and Reduction, Version 6.02, Bruker AXS, Inc., Madison, WI, 2002.
[18] SADABS, Software for Empirical Absorption Correction, Version 2.03, Bruker AXS, Inc., Madison, WI, 2002.
[19] G.M. Sheldrick, SHELXTL, Program for Crystal Structure Refinement, University of Gottingen, Gottingen, Germany, 1997.
[20] K. Nakamoto, Infrared Spectra and Raman Spectra of Inorganic and Coordination Compounds, John Wiley & Sons, New York, 1986.
[21] M. Kurmoo, C. Estournes, Y. Oka, H. Kumagai, K. Inoue, Inorg. Chem. 44 (2005) 217.
[22] M.D. Allendorf, C.A. Bauer, R.K. Bhakta, R.J.T. Houk, Chem. Soc. Rev. 38 (2009) 1330 (and references therein).
[23] M.E. Fisher, Am. J. Phys. 32 (1964) 343.